de Haas–van Alphen Effect in Antimony-Tin Alloys*

A. E. Dunsworth and W. R. Datars
Department of Physics, McMaster University, Hamilton, Canada
(Received 3 October 1972)

The de Haas–van Alphen (dHvA) effect was used to measure the Fermi surfaces of pure antimony and antimony alloys with up to 0.29-at.% tin. At the highest concentration, the hole dHvA frequencies increased by 75% and the electron frequencies decreased to less than half of the pure-antimony values. Cyclotron masses of electrons and holes at absolute frequency minima increased and decreased for holes and electrons, respectively, giving a definite indication of nonparabolic conduction and valence bands. A comparison of the hole- and electron-Fermi-surface volumes with the number of tin atoms added showed that one tin atom removes one electron from the alloy as expected from the unit valence difference between antimony and tin. This result corrects that found by other workers using different techniques. Extrapolation of the hole and electron densities in the alloys indicates that the electron pocket will be empty at ~0.35-at.% tin while the hole pocket will disappear at about the same concentration of a hexavalent element such as tellurium. The rigid-band predictions without any corrections for changes of lattice parameter describe the observed frequency shifts quite well at low concentrations. At higher values there is a deviation caused by the mass and Fermi-surface-shape changes. The Fermi-surface shape and cyclotron mass are also discussed in terms of a band structure determined from the Falicov–Lin pseudopotential.

I. INTRODUCTION

Extensive studies of the Fermi surface of pure antimony (Sb)[1–5] considered in light of the pseudopotential band structure of Falicov and Lin[6] indicate that there are three electron pockets centered at the L point of the Brillouin zone along with six hole pockets centered at H near the T point. Each pocket is roughly ellipsoidal with deviations that can be measured experimentally.[1,2,7] There are 5.5×10^{19} electrons/cm^3 with an equal number of holes. The present work explores the band structure near the Sb Fermi level by changing the Fermi level by doping with tin (Sn).

The present work was undertaken to determine how the Fermi surface of antimony alloyed with a small amount of tin differed from the pure-antimony Fermi surface and whether the differences observed were in agreement with theories of alloying, particularly the rigid-band theory. Previously, galvanomagnetic studies have been made on antimony alloys with less than 0.8-at.% tin[3] and for concentrations between 2- and 8-at.% tin.[8] Also Ishizawa and Tanuma[9] took de Haas–van Alphen (dHvA) measurements on a 0.1-at.%-tin alloy. These authors indicated that the band shapes do not change greatly with alloying. The Fermi surface increased and decreased for holes and electrons, respectively. However, such measurements were not very sensitive to the detailed shape of the Fermi surface, in contrast with the high sensitivity to shape of a detailed dHvA experiment. This previous work suggested that only 0.3 electrons per atom were removed by adding tin, a value much smaller than the valence difference of one between antimony and tin. Theoretically such a large discrepancy was not expected.

In the description of the experimental method in Sec. II, attention is given to the care used in the preparation and annealing of the alloys; it also describes a method of determining cyclotron mass from Fourier components even with several dHvA frequencies present. Experimental results in Sec. III give dHvA frequencies and cyclotron masses for directions in the trigonal-bisectrix and trigonal-binary planes of Sb and five alloys. In Sec. IV the rigid-band model, changes in band shape with alloying, and nonrigid bands are discussed in separate parts. Section V consists of a summary and conclusions.

II. EXPERIMENTAL

The alloys were prepared from high-purity Sb and Sn in a carbon-coated Vycor tube. A horizontal zone-leveling procedure[10] was used to mix the elements and grow large single crystals. Annealing had a large effect on the dHvA frequencies. Unannealed alloys showed a much smaller change of dHvA frequency from pure Sb than annealed samples. A check of the frequencies after annealing for one and two weeks indicated that one week was sufficient for good solution of Sn in Sb. The alloys for which results are reported were annealed for one week at 600 °C.

Single crystals were spark cut from ingots and were oriented by x rays in the trigonal-binary and trigonal-bisectrix plane. The samples were analyzed by atomic absorption which gave values of

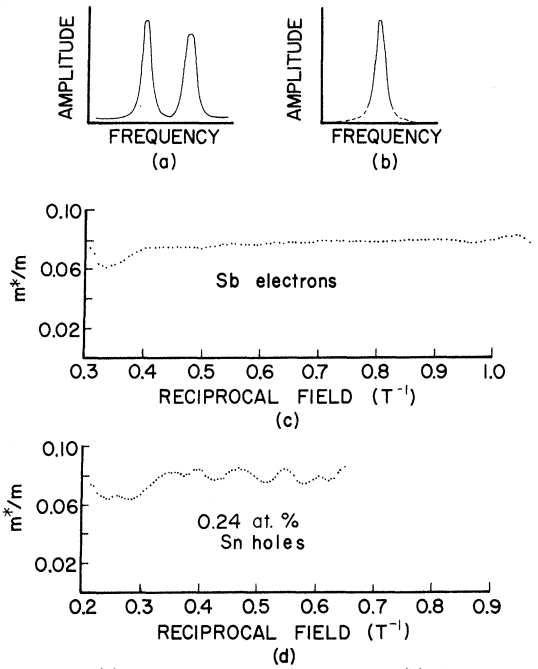

FIG. 1. (a) Two dHvA Fourier peaks; (b) the spectrum with one peak removed and the resulting discontinuities replaced by extrapolated tails (dashed lines) of the frequency distribution; (c) cyclotron mass of pure antimony as a function of reciprocal magnetic field; (d) cyclotron mass for 0.24-at.% Sb(Sn) alloy as a function of reciprocal magnetic field.

0.037 ± 11%, 0.17 ± 5%, 0.23 ± 1.5%, 0.24 ± 1%, and 0.29 ± 1% at.%. These numbers are approximately 50% lower than the nominal concentrations of Sn added to the ingot. Alloys with 0.42 and 0.51 at.% were made but did not show the dHvA effect.

The dHvA experiments were done with the sample in a 55-kOe Westinghouse superconducting magnet by the low-frequency-modulation technique. The data were collected on magnetic tape and Fourier analyzed by computer.[11] The cyclotron mass was found from the temperature dependence of the dHvA amplitude. A Texas Instruments precision pressure gauge was used to measure the liquid-helium vapor pressure.

The cyclotron masses were calculated by separating the sine and cosine Fourier components of several dHvA oscillations as shown in Fig. 1. Figure 1(a) shows two nearby dHvA frequencies. Figure 1(b) shows one frequency removed and the "tails" of the peak replaced by a frequency-dependent function to eliminate discontinuities in the function values. An inverse Fourier transform restored the original dHvA frequency and envelope function without any interference from the other frequency component. The function

$$f(m^*, H) = \sum_i \left(\frac{y_i T_0}{y_0 T_i} - \frac{\sinh(\alpha m^* T_0/H)}{\sinh(\alpha m^* T_i/H)} \right)^2 \qquad (1)$$

was minimized to find the least-squares value of the cyclotron mass m^*. The parameter α is defined to be $2\pi^2 k_B/e\hbar$. In Eq. (1), y_i and y_0 are the amplitudes of the dHvA oscillations at temperatures T_i and T_0, respectively. Figures 1(c) and 1(d) are typical results showing the ratio of the cyclotron mass to the free-electron mass m^*/m, vs $1/H$ for two samples. The frequency resolution and signal-to-noise ratio is somewhat poorer in the alloy than in pure Sb. The deviation near the upper and lower limits comes from the inverse Fourier transform, indicating that the discontinuity mentioned above has not been completely smoothed out. The mass values presented are an average over magnetic field except for the 0.29-at.% values. The electron and hole masses at this concentration were determined from a few oscillations on a strip-chart recorder without any Fourier analysis. The Dingle temperature was found in a similar way by calculating the slope of

$$\ln\left(\frac{y_i (H^{1/2}) \sinh(\alpha m^* T/H)}{T_i J_2(2\pi F h/H^2)} \right)$$

vs $1/H$, where F is the dHvA frequency, h is the modulation-field amplitude, and J_2 is the Bessel function.

III. EXPERIMENTAL RESULTS

Measurements were taken with the magnetic field in the trigonal-binary and trigonal-bisectrix planes of each alloy. The cyclotron masses and Dingle

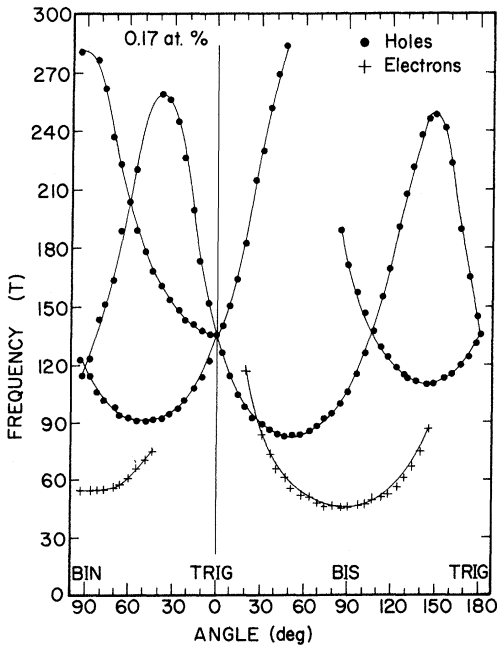

FIG. 2. dHvA frequencies for 0.17-at.% Sb(Sn) alloy for field directions in the trigonal-bisectrix and trigonal-binary planes.

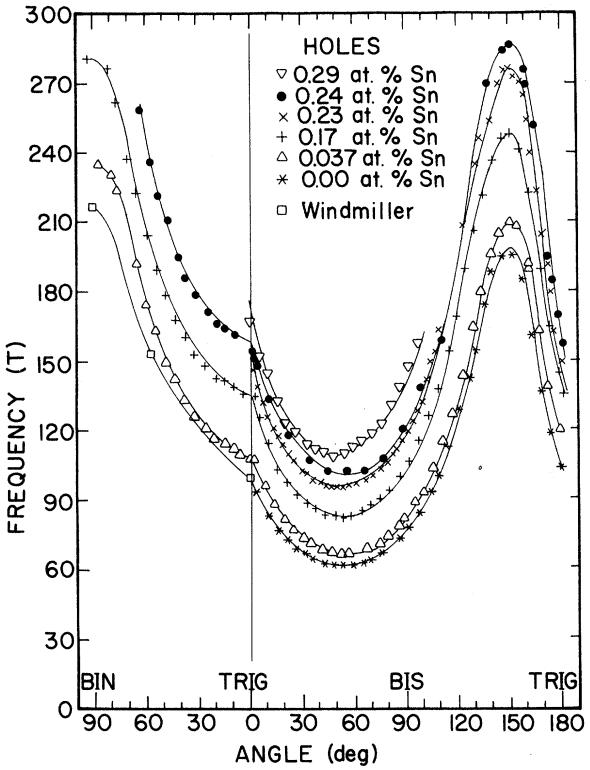

FIG. 3. Principal hole frequencies vs field directions in the binary- and bisectrix-trigonal planes for Sb and Sb(Sn) alloys.

temperatures were found at the electron and hole minima in the trigonal-bisectrix plane. Figure 2 shows a typical dHvA frequency versus angle plot with harmonic and sum frequencies removed. Figures 3 and 4 show data of the principal branches of holes and electrons, respectively, for the different samples. The electron frequencies decrease to less than half the Sb value while the hole frequencies increase by 75% with the addition of 0.29-at.% Sn. The surfaces are nearly ellipsoidal in shape, as suggested by the data, but closer examination indicates that the hole-surface maximum and minimum in the trigonal-bisectrix plane are not 90° apart as required for an ellipsoid but actually are 95° apart. There is no significant shift of the tilt angles of the Fermi-surface pockets with concentration, but there is a slight change in the axial ratio of the hole surface. The maximum-to-minimum frequency ratio in the trigonal-bisectrix plane decreases to 2.8 at 0.24-at.% Sn from the value of 3.2 in Sb. Our experiments were unable to resolve the higher-frequency regions of the electron branches and no conclusions about the change of shape of the electron pockets with alloying can be made.

Each mass value is an average over field, as shown in Figs. 1(c) and 1(d). Fifteen to seventeen values of temperatures between 4.2 and 1.2 °K were used to find a mass and Dingle temperature. The concentration dependence of the cyclotron mass is shown in Fig. 5.

Table I summarizes the data at important places in the trigonal-binary and trigonal-bisectrix planes. The hole mass increases with increasing concentration while the electron mass decreases. The Dingle temperature rises with concentration for both holes and electrons. The frequency values of pure Sb are in excellent agreement with Windmiller's results.[1] The mass values for Sb are a few percent lower for both electron and holes.

IV. DISCUSSION

A. Rigid-Band Model

When a small number of impurities are added to a pure metal, the rigid-band model assumes that no change will occur in the band structure and states that the electron concentration will be raised or lowered by ZCN_0, where Z is the valence difference between host and impurity, C is the atomic concentration of impurities, and N_0 is the number of host atoms per cm^3. This can be expressed

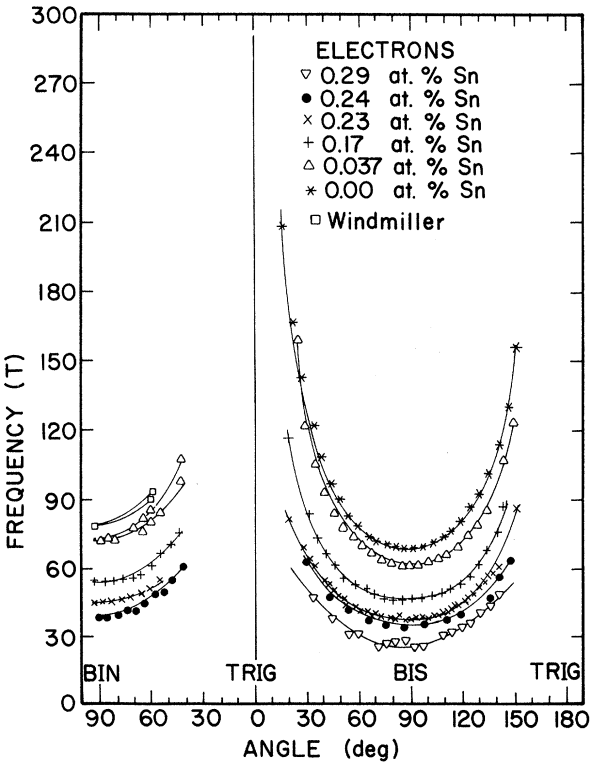

FIG. 4. Principal electron frequencies vs field direction in the binary- and bisectrix-trigonal planes for Sb and Sb(Sn) alloys.

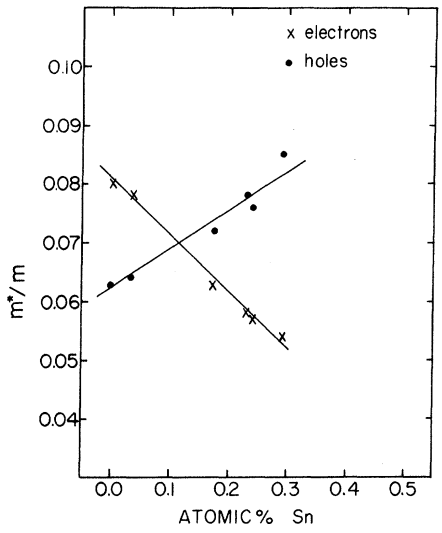

FIG. 5. Dependence of cyclotron mass on tin concentration at electron and hole minima.

more exactly[12] by writing the change of Fermi energy ΔE as

$$\Delta E = ZC/D_0(E_F)\,, \tag{2}$$

where $D_0(E_F)$ is the density of states in the pure metal at the Fermi energy E_F. It should be pointed out that this expression assumes that ΔE is small and $D_0(E_F)$ is not strongly energy dependent. Heine[12] defines a parameter

$$R = \frac{A - A_0}{A_0 ZC} = \pm \frac{mc}{\hbar e} \frac{m_0^*}{F_0 D_0(E_F)}\,, \tag{3}$$

where $A - A_0$ is the change of Fermi surface area from the area A_0 of the pure metal, and F_0 and m_0^* are the dHvA frequency and cyclotron mass in the pure metal. The cyclotron mass m^* is defined by

$$m^* = \frac{\hbar^2}{2\pi}\left(\frac{\partial A}{\partial E}\right)_{E_F}\,. \tag{4}$$

In deriving Eq. (3), $A - A_0$ and ΔE have been related through Eq. (4). If m^* is a function of E_F, Eq. (3) is only approximately correct. If $A - A_0$ is expanded in a Taylor series in E up to second order, then

$$R = \pm \frac{mc}{\hbar e} \frac{m_0^*}{F_0 D_0(E_F)} \left(\frac{m_0^* + m^*(C)}{2m_0^*}\right)\,, \tag{5}$$

where $m^*(C)$ is the mass of the alloy. If $m^*(C) = m_0^*$, Heine's result [Eq. (3)] is obtained. The $\pm$ signs in Eqs. (3) and (5) indicate whether the Fermi-surface area increases or decreases on alloying. We compare the rigid-band model with experiment by plotting $(F - F_0)/F_0$ against C and rearranging Eq. (3) to give

$$(F - F_0)/F_0 = 1.85 \times 10^5 (Zm_0^* C/F_0)\,.$$

TABLE I. dHvA frequencies, cyclotron masses, and Dingle temperatures in Sb-Sn alloys.

Tin concentration (at. %)	0.00	0.035	0.17	0.23	0.24	0.29
Minimum electron frequency (T) in trigonal-bisectrix plane	68	61	46.5	38	34	26
Cyclotron-mass electron minimum (free-electron mass)	0.080	0.078	0.063	0.058	0.057	0.054
Dingle-temperature electron minimum (°K)	2.9	4.5	7.6	•••	8.5	•••
Minimum hole frequency (T) in trigonal-bisectrix plane	61.5	67	83	95	101	109
Cyclotron-mass hole minimum (free-electron mass)	0.063	0.064	0.072	0.078	0.076	0.085
Dingle-temperature hole minimum (°K)	2.5	3.3	6.2	•••	11.5	•••
Maximum hole frequency (T) in trigonal-bisectrix plane	197	211	249	271	287	•••
Maximum hole frequency (T) in trigonal-binary plane	216	234	281	•••	•••	•••

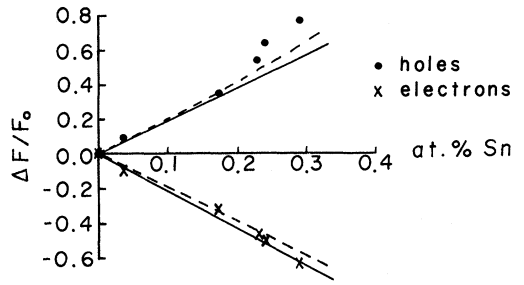

FIG. 6. Comparison of observed relative frequency shifts with rigid-band theory. Solid lines are calculated from the simple rigid-band model of Eq. (3). Dashed lines are predicted by the mass-dependent model, Eq. (5).

A value of $D_0(E_F) = 4.67 \times 10^{-2}$ (atom/eV)$^{-1}$ determined from the electronic specific-heat constant[13,14] was used. A plot of $(F - F_0)/F_0$ vs concentration is presented in Fig. 6 where the rigid-band predictions of Eq. (3) are shown by the solid lines. The dashed lines are the results predicted by the mass-dependent R of Eq. (5). The agreement is quite good for the electron branch and at the lower concentrations of the hole branch but deviates somewhat for the three highest concentrations of the hole branch. Part of this deviation is due to the mass and shape change found for this band.

The change of total carrier concentration was calculated from the dHvA frequencies using the ellipsoidal approximation. For the hole surface, the three extremal frequencies were found from the data. For the electron surface, it was assumed that the relative axial ratios remained the same as in pure antimony so that the volume of the Fermi surface could be scaled as the three-halves power of the ratio of the minimum alloy and antimony frequencies. Table II shows the carrier densities, total change of carrier density, the number of tin atoms added, and the ratio of the carrier-density change to the tin density. The last row indicates that all the tin atoms added are effective in changing the carrier concentration. The average value of carrier-density change to tin-atom density is 1.02, quite close to the rigid-band prediction of 1.00. A combination of error in the tin concentrations and the approximations made in calculating the electron volume probably accounts for the observed difference from 1. If the rigid-band model holds, the results suggest that the electron pocket has been slightly underestimated in size, indicating that the axial ratio increases slightly with concentration. The fact that the number of carriers agrees quite well with the rigid-band model implies that the deviation found in Fig. 6 is caused by changes not accounted for by the simple rigid-band model. It appears that Ishizawa and Tanuma[9] had less tin in their sample than they thought because the change in frequency is too small for their stated concentration according to our results. Also, Epstein and Juretschke[3] found that tin removes 0.3 electrons per atom, less than that found here. No evidence of an extra set of holes as suggested by Saunders and Oktu[8] was found. This is not too surprising since the concentrations of our alloys were considerably less. Extrapolation of our change of electron density with alloying indicates that the electron pocket will be empty at ~0.35-at.% Sn. This contradict previous workers[3,15] who suggested from 1 to 2 at.% is required. Finally, when our results are extrapolated to the case of antimony doped with atoms of valence 6 such as tellurium, it is suggested that the hole carriers in the valence band will disappear at approximately 0.35 at.%.

B. Band Shapes

Three types of bands will be considered: the ellipsoidal-parabolic band,[16] the ellipsoidal-nonparabolic Kane band,[17] and finally a pseudopotential band.

The ellipsoidal-parabolic band has the well-known form (E in Ry, k in a.u.)

$$E = \frac{k_x^2}{m_1} + \frac{k_y^2}{m_2} + \frac{k_z^2}{m_3} \quad ,$$

which gives ellipsoidal Fermi surfaces and energy-independent cyclotron masses. This band can be taken as a first approximation to the actual Fermi surface of Sb to describe the gross features. However, it does not predict any change of shape with energy, observed nonellipsoidal behavior, or the observed energy-dependent cyclotron mass. This band does enable certain calculations to be made easily, such as the carrier concentration, and will be useful later in the calculation of the overlap of energy bands.

The ellipsoidal-nonparabolic band has the form

TABLE II. Carrier densities in Sb-Sn alloys and change of density from that of pure Sb.

Tin concentration (at.%)	0.00	0.035	0.17	0.23	0.24	0.29
Number of Sn atoms (10^{19} cm^{-3})	0.0	1.2	5.7	7.6	7.9	9.6
Number of electrons (10^{19} cm^{-3})	5.55	4.74	3.11	2.08	1.96	1.58
Number of holes (10^{19} cm^{-3})	5.52	6.18	8.19	9.61	10.2	11.1
Total change of carrier density (10^{19} cm^{-3})	···	1.44	5.08	7.53	8.24	9.5
Total change/ number of Sn atoms	···	1.20	0.89	0.99	1.04	0.99

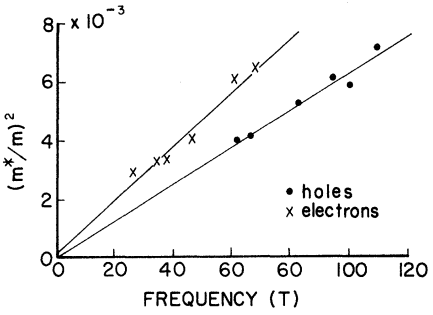

FIG. 7. Square of the cyclotron mass of electrons and holes as a function of dHvA frequency compared with least-squares–fitted lines predicted by nonparabolic bands.

$$E+\frac{E^2}{E_g}=\frac{k_x^2}{m_1}+\frac{k_y^2}{m_2}+\frac{k_z^2}{m_3} \quad ,$$

where E_g is the energy gap separating this band from another band near it. If E_g is large, it is obvious that the ellipsoidal-parabolic band is restored. However, in the case of Sb and its alloys, there is reason to expect that both hole and electron bands will interact with neighboring bands having nearly the same energy.[6]

The energy surfaces for this band are again ellipsoids but the cyclotron mass in now energy dependent. The cyclotron mass for an orbit in the xy plane is given by

$$m^*=m_b(1+2E/E_g)\,, \tag{6}$$

where m_b is the band-edge mass. The cross-sectional area is

$$A=\pi m_b(1+E/E_g)E\ . \tag{7}$$

Equations (6) and (7) can be combined to give

$$m^{*2}=m_b^2+(4/\pi)A\,(m_b/E_g)\ . \tag{8}$$

Since A is directly proportional to the dHvA frequency, Eq. (8) can be tested experimentally for the electron and hole minima as shown in Fig. 7. The fitted least-squares line has a negative intercept for holes and a positive intercept for electrons. The scatter of the data points gives little meaning to the intercept value. The slope of the lines is more accurately determined and gives a value of the $\vec{k}\cdot\vec{p}$ matrix element E_p $(=E_g/m_b)$. The matrix element is 7.3 eV for holes and 5.0 eV for electrons. These values compare with 20 eV for III-V semiconductors[18] and 8 eV for bismuth-antimony.[19] The ellipsoidal nonparabolic model describes the mass changes reasonably well and gives some insight into the band interactions, but it cannot explain the deviation from ellipticity or change of axial ratio with concentration. To incorporate these nonellipsoidal nonparabolic features in one model, we carried out pseudopotential band-structure calculations.

The pseudopotential model is based on the work of Falicov and Lin[6] for pure antimony, diagonalizing an 89×89 determinant to find the Fermi surface and energy bands. We used the same pseudopotential to examine the hole and electron Fermi surfaces in more detail.

A grid of points was chosen in $\vec{k}$ space around each pocket center and energy values were found for each point. Two examples of the grid in the mirror plane are shown in Figs. 8 and 9. Since the electron pocket has inversion symmetry only half the surface is needed. The dividing line corresponds to the Brillouin-zone boundary. The hole band is separated from a nearby band by the spin-orbit interaction with a spin-orbit constant of 0.02 Ry. Other grids parallel to the ones shown were obtained to describe the Fermi surface away from the mirror plane. Both surfaces are approximately ellipsoidal, as expected. More exact comparisons were made by expanding the energy E in a power series in k up to fourth order and fitting this series to the grid points. In this way, cross-sectional areas and cyclotron masses were calculated numerically for any orientation. Fourteen parameters were used to describe the electron surface and 22 for the hole surface. The extremal hole surface

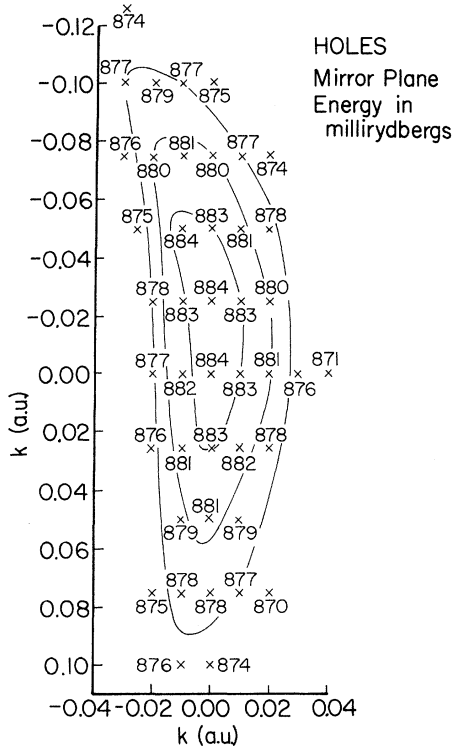

FIG. 8. Pseudopotential-hole-energy grid in the trigonal-bisectrix mirror plane.

areas are not central and a search was made for the maximum area corresponding to the dHvA frequency. The results are summarized in Table III. The Fermi energy E_F is referred to the band edge, and concentrations were estimated from a comparison of the calculated minimum areas with the data. The alloy calculations were made by changing the Fermi energy to fit measured dHvA frequencies. This is using a rigid-band approach to alloying.

The theoretical hole surface does not describe the observed surface very well. The theoretical frequency ratios are too large, making the calculated carrier density 25% too large. The calculated masses are twice the observed values and do not show much change with concentration. The model does predict a shape change of nearly the percentage found from the data.

The theoretical electron surface agrees more closely. The masses are nearly the right size and show the downward trend with concentration found experimentally. The frequency ratio increases very slightly with concentration. In Falicov and Lin's original paper, it was noted that the electron surface was described much better by the pseudopotential than was the hole surface. Part of this is attributed to the difficulties of calculation when the pocket has no inversion symmetry.

TABLE III. Results of a pseudopotential calculation of the Fermi surface of Sb and Sb (Sn) alloys in the trigonal-bisectrix plane.

	Holes		Electrons	
Tin concentration	0.00	0.23	0.00	0.23
Fermi energy (Ry)	0.003	0.006	0.010	0.006
Minimum frequency (T)	57	95	68.5	37
Maximum frequency (T)	248	375	427	234
Cyclotron mass at minimum (m^*/m)	0.14	0.13	0.073	0.060
Ratio of theoretical maximum and minimum frequency	4.4	4.0	6.2	6.3
Ratio of observed maximum and minimum frequency	3.2	2.8	...	...

C. Nonrigid Bands

We have investigated some possibilities for nonrigid bands. The ellipsoidal-parabolic model was used to estimate the band overlap energy E_0 defined as the sum of the hole and electron Fermi energies. E_0 is constant within experimental error for all the alloys with a value of 0.016 Ry, indicating that the bands are rigid. This value compares favorably with 0.013 Ry found from the pseudopotential calculations.

The energy shifts of the centers of the pseudopotential bands were calculated allowing for changes of lattice constant and pseudopotential on alloying to check the rigid-band model in the pseudopotential calculation. The alloy lattice constants were taken from Refs. 20 and 21 except for the internal displacement parameter which was estimated from Ref. 22. The energy shifts found were ~0.0008 Ry/at.% Sn. These are insignificant for concentrations of 0.8 at.% or less.

A final comparison was made with the scattering theory of Soven.[23] We calculated the difference potential from the pseudopotentials of Sb and Sn and estimated the s-wave phase shift δ_0 from the Born approximation and a numerical solution of the scattering equation. Our value of $\delta_0 = 0.1$ with Soven's results predicts a 20% reduction in Fermi energy from the rigid-band prediction. This reduction was not observed.

V. SUMMARY AND CONCLUSIONS

The hole and electron energy bands of pure antimony and antimony-tin alloys with up to 0.29-at.% Sn have been studied using the dHvA effect. At the highest concentration, the hole frequencies increased by 75% over the pure-antimony values while the electron frequencies were reduced to less than half their original sizes. The cyclotron masses were found from the temperature dependence of the amplitude at the principal hole-and electron-branch minima.

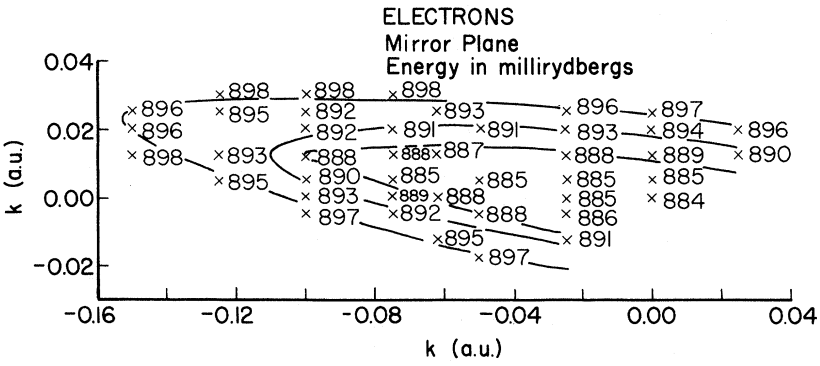

FIG. 9. Pseudopotential-electron-energy grid inside the Brillouin-zone boundary in the trigonal-bisectrix mirror plane.

The hole mass increased by 35% while the electron mass decreased by about 32%. This gives a direct indication of nonparabolic conduction and valence bands. The Dingle temperature increased by a factor of 3 above the pure-antimony value of ~ 2.5 °K. The increase is roughly linear with concentration. The rigid-band predictions without any corrections for changes in lattice parameter describe the observed frequency shifts quite well at low concentrations. At higher values there is a deviation caused by the mass and Fermi-surface shape change. Estimates of the Fermi-surface volume allow us to find the hole and electron carrier concentrations in each alloy. The results show that each tin atom removes one electron from the alloy. This value is in agreement with the valence difference between Sb and Sn and is greater than that found by previous workers. If the electron and hole carrier densities are extrapolated to higher Sn concentrations our data suggest that the electron pocket disappears at ~ 0.35-at.% Sn while the hole pocket disappears at ~ 0.35 at.% of a hexavalent element such as tellurium.

Various features of the data have been related to different band models. A Kane ellipsoidal-nonparabolic band was used to describe the mass change with concentration. The $\vec{k} \cdot \vec{p}$ matrix element deduced from the data was 7.3 eV for holes and 5.0 eV for electrons. The mass and shape changes were compared with the Falicov–Lin[6] band-structure calculation in pure antimony. The electron band of the alloy is much better described by this model than is the hole band. A calculation based on the ellipsoidal-parabolic model indicates that the band overlap is constant throughout out concentration range. An estimate of the scattering phase shift was found from the pseudopotential difference of antimony and tin and was used to predict the deviation from rigid-band behavior as calculated by Soven.[23] The theoretical deviation was larger than that observed experimentally.

ACKNOWLEDGMENTS

The authors wish to thank Y. Ishizawa and R. Jenkins for useful suggestions and discussions and C. Verge for technical assistance.

---

*Work supported by the National Research Council of Canada and the Defence Research Board.

[1]L. R. Windmiller, Phys. Rev. 149, 472 (1966).

[2]W. R. Datars and J. Vanderkooy, IBM J. of Res. Develop. 8, 247 (1964).

[3]S. Epstein and A. J. Juretschke, Phys. Rev. 129, 1148 (1963); K. Tanaka, S. K. Suri, and A. L. Jain, Phys. Rev. 170, 664 (1968).

[4]C. Nanney, Phys. Rev. 129, 109 (1963); M. S. Dresselhaus and J. G. Mavroides, in *Optical Properties and Electronic Structure of Metals and Alloys*, edited by B. Abeles (North-Holland, Amsterdam, 1966), p. 508.

[5]R. D. Herod, C. A. Gage, and R. G. Goodrich, Phys. Rev. B 4, 1033 (1971).

[6]L. M. Falicov and P. J. Lin, Phys. Rev. 141, 562 (1966).

[7]J. B. Ketterson and L. R. Windmiller, Phys. Rev. B 1, 463 (1970).

[8]G. A. Saunders and O. Oktu, J. Phys. Chem. Solids 29, 1589 (1968).

[9]Y. Ishizawa and S. Tanuma, J. Phys. Soc. Japan 20, 1279 (1965).

[10]W. G. Pfann, *Zone Melting* (Wiley, New York, 1966).

[11]R. G. Poulsen, J. S. Moss, and W. R. Datars, Phys. Rev. B 3, 3107 (1971).

[12]V. Heine, Proc. Phys. Soc. (London) A69, 505 (1954).

[13]D. C. McCallum and W. A. Taylor, Phys. Rev. 156, 782 (1967).

[14]N. H. Zebouni and R. S. Blewer, Phys. Letters A 24, 106 (1967).

[15]S. H. Browne and C. T. Lane, Phys. Rev. 60, 895 (1941).

[16]H. Jones, Proc. Roy. Soc. (London) A155, 653 (1936).

[17]B. Lax, J. G. Mavroides, W. J. Zeiger, and R. J. Keyes, Phys. Rev. Letters 5, 241 (1960); E. O. Kane, J. Phys. Chem. Solids 1, 249 (1957).

[18]H. Ehrenreich, J. Appl. Phys. (Suppl.) 32, 2155 (1961).

[19]M. R. Ellett, R. B. Horst, L. R. Williams, and K. F. Cuff, J. Phys. Soc. Japan 21, 666 (1966).

[20]G. Hagg and A. G. Hybinette, Phil. Mag. 20, 913 (1935).

[21]E. G. Bowen and W. M. Jones, Phil. Mag. 12, 441 (1931).

[22]B. Morosin and J. E. Schirber, Phys. Letters A30, 512 (1969).

[23]P. Soven, Phys. Rev. B 5, 2, 260 (1972).